Chemical Science

ROYAL SOCIETY OF CHEMISTRY

EDGE ARTICLE

View Article Online
View Journal

Cite this: DOI: 10.1039/d6sc00779a

All publication charges for this article have been paid for by the Royal Society of Chemistry

Convenient large-area construction of flexible multicolor polymer-based room temperature phosphorescence materials with second-scale phosphorescence lifetimes

Tianyu Li,†[a] Yan Zhu,†[a] Shaochen Sun,[a] Yutong Zhou,[a] Zhihui Wang,[a] Fei Li,[b] Farong Tao,*[a] Liping Wang [a] and Guang Li *[a]

Received 28th January 2026
Accepted 9th February 2026

DOI: 10.1039/d6sc00779a

rsc.li/chemical-science

The preparation of multicolor organic room temperature phosphorescence (RTP) materials with flexibility and second-scale phosphorescence lifetime is highly attractive yet remains extremely challenging. Here, we synthesize a series of carbazole-functionalized polyacrylamide copolymers P(AM-*co*-VBC) by free radical copolymerization, which can show up to 20 s of a bright blue afterglow accompanied by 3.720 s of the RTP lifetime. After water-dissolution and drying treatments, the bright blue afterglow of W-P(AM-*co*-VBC) visible to the naked eye is extended to 43 s, while the longest RTP lifetime increases to 4.664 s due to the self-assembly of carbazole group aggregates inducing an aggregation-induced emission enhancement effect. Using W-P(AM-*co*-VBC) as an energy donor and commercially available fluorescent dyes as energy acceptors, multicolor RTP materials are facilely prepared through a phosphorescence Förster resonance energy transfer strategy. Notably, flexible multicolor RTP films with high transparency and long RTP lifetime are conveniently fabricated over large areas by doping the multicolor RTP materials into sodium alginate matrices with trace amounts of poly(vinyl alcohol) as a regulator. Furthermore, the prepared multicolor ultralong RTP materials demonstrate significant potential for advanced applications in the fields of information encryption and flexible display.

Introduction

Organic room temperature phosphorescence (RTP) materials have attracted significant attention in the fields of sensing,[1–3] data encryption,[4–6] bioimaging,[7–9] and organic light-emitting diodes.[10,11] However, the majority of reported organic RTP materials are currently based on crystalline small molecules.[12,13] The drawbacks of small molecule-based RTP materials that cannot be easily processed and prepared into devices limit their application scope to some extent, and these limitations provide impetus for the development of alternative organic RTP materials. Excitingly, due to their advantages such as low cost, low toxicity, ease of modification, good processability, and suitability for device fabrication, polymer-based RTP materials have become another research hotspot.[14–18] The unique long-chain structure of polymers not only effectively suppresses the movement of the phosphor molecules, but also mitigates the quenching effects of environmental oxygen and moisture, thereby promoting RTP emission.[19–21] The selection of the polymer matrix is crucial for constructing polymer-based RTP materials. To date, several polymers, including polylactic acid,[22] polyacrylamide (PAM),[23,24] poly(methyl methacrylate),[25–27] poly(-vinyl alcohol) (PVA),[28–30] and polyacrylic acid[31–33] have been adopted as ideal matrices. Doping small organic luminophores into polymer matrices and covalently bonding small organic luminophores to polymer chains are the main strategies for preparing polymer-based RTP materials.[34–37] However, physical doping systems often suffer from phase separation, which weakens RTP performance. In contrast, covalent bonding between small organic molecule luminophores and polymer chains can form a more stable structure, facilitating efficient RTP emission. Despite this advantage, the covalent bonding strategy remains less explored for polymer-based RTP materials because of the inherent complexity of the synthesis procedures.[18,38] To the best of our knowledge, polymer-based RTP materials with phosphorescence lifetime exceeding 1 s remain relatively scarce.[39,40]

Multicolor organic RTP materials have great application prospects in multicolor display, polychromatic imaging and anti-counterfeiting.[41–46] Several strategies including designing the structure of phosphor molecules from different electron donating/accepting abilities or π-conjugation degrees,[47,48]

[a]School of Materials Science and Engineering, Liaocheng University, Liaocheng 252059, China. E-mail: taofarong@lcu.edu.cn; lglzsd@126.com

[b]College of Chemistry, Chemical Engineering and Materials Science, Shandong Normal University, Jinan 250014, China

† These authors contributed equally to this work.

regulating molecular arrangement in the crystalline state,[49] fabricating multiple phosphorescence emission centers,[50,51] and controlling the Förster resonance energy transfer (FRET) process,[52] have been developed for constructing multicolor RTP materials. Due to its simplicity and feasibility of the preparation process, the FRET strategy is particularly advantageous for preparing polymer-based multicolor RTP materials. The match between the energy donor and acceptor critically influences the FRET efficiency, thereby significantly affecting the duration of afterglow. Wang *et al.* achieved color-tunable long persistent luminescence *via* phosphorescence FRET in three-component doping PVA systems, using indolocarbazole isomers as energy donors and commercially fluorescent dyes as acceptors.[53] Peng *et al.* doped a series of fluorescent emitter guests with varied emissive colors into PAM-based RTP host materials to achieve full-color afterglow from blue to red and even white *via* the FRET process.[54] However, despite its potential, the preparation of multicolor polymer-based RTP materials with ultralong afterglow time by the FRET strategy remains challenging, particularly due to the difficulty in optimizing donor–acceptor pairs and achieving efficient energy transfer.

The reported organic RTP materials including polymer-based RTP systems are mostly in the form of crystals, powders or hard flakes, which greatly hinders their flexible applications. Because some polymers possess inherent flexibility, their use as matrices for constructing flexible RTP materials has attracted much attention.[55–58] Ju *et al.* prepared stretchable PAM hydrogels with unique RTP properties by polymerization-induced crystallization of dopant dibenzo-24-crown-8-ether molecules.[59] Wei *et al.* fabricated a full-color flexible RTP material by doping different colored PAM-based RTP materials and PVA into a polydimethylsiloxane matrix.[60] Despite the breakthroughs in the research of polymer-based flexible RTP materials, in-depth development of multicolor and flexible RTP materials with extremely long afterglow under environmental conditions is urgently needed due to their vast application prospects.

Herein, flexible polymer-based multicolor RTP materials with second-scale phosphorescence lifetime are facilely prepared over large areas through a convenient doping-coating method in combination with a phosphorescence FRET strategy. A series of ultralong RTP materials P(AM-*co*-VBC) with the longest bright blue afterglow of 20 s and the longest phosphorescent lifetime of 3.720 s are synthesized by radical copolymerization of acrylamide (AM) with 9-(4-vinylbenzyl)-9*H*-carbazole (VBC). Impressively, after water-dissolution and drying treatment, the afterglow duration of W-P(AM-*co*-VBC) increases to 43 s, accompanied by an unexpectedly extended RTP lifetime of up to 4.664 s. Multicolor RTP materials are developed by doping commercially available fluorescent dyes fluorescein (FL), calcein (CAL), rhodamine 6G (R6G), and sulforhodamine B (SRB) as energy acceptors into the W-P(AM-*co*-VBC) donor matrix. Interestingly, color-tunable persistent afterglow emissions from cyan to yellow, pink, and purple with exciting RTP lifetimes of as high as 3.837, 2.416, 2.452, and 1.993 s are realized through efficient phosphorescence FRET. By blending ultralong multicolor P(AM-*co*-VBC)-based RTP materials into an environmentally friendly natural polymer matrix sodium alginate (SA) mixed with trace amounts of PVA, colorful and flexible RTP films with phosphorescence lifetimes of more than 1 s are successfully fabricated over large areas using a simple doping-coating-drying process (Scheme 1). Moreover,

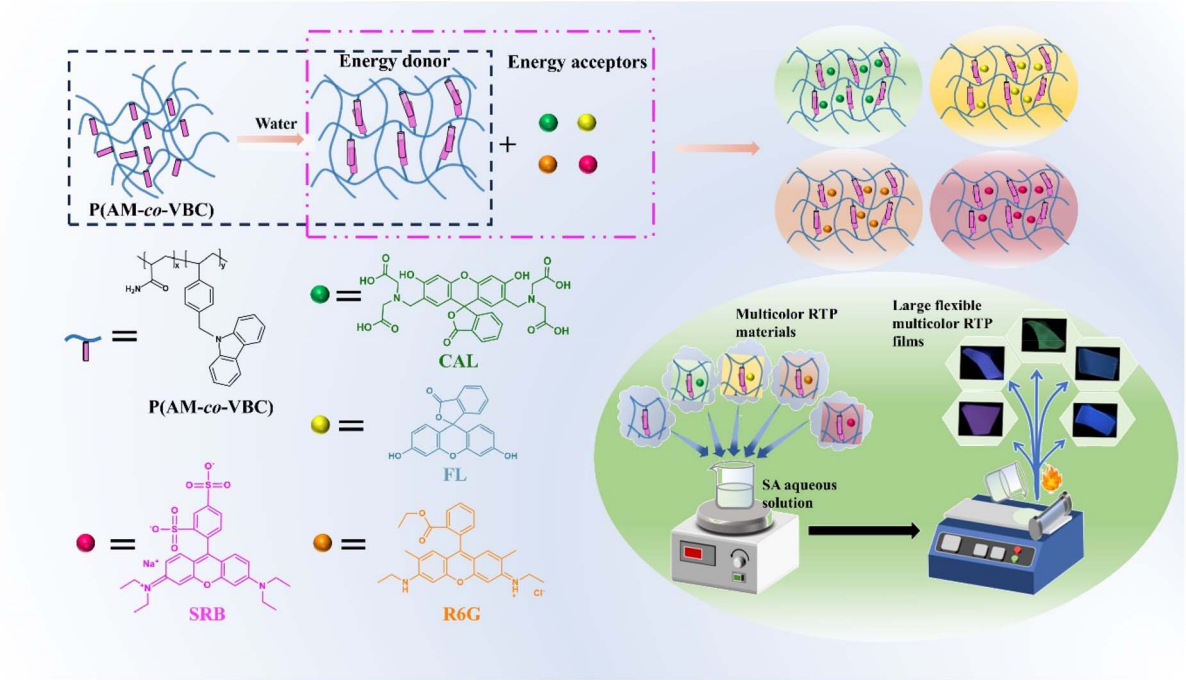

Scheme 1 Schematic representation of multicolor RTP materials and flexible multicolor RTP films.

taking advantage of ultralong afterglow, multicolor, and flexibility, the prepared RTP materials exhibit potential application value in information encryption and multicolor flexible display. This work provides an efficient and facile way to guide the large-area construction of flexible multicolor RTP materials with ultralong lifetimes.

Results and discussion

Photophysical properties of P(AM-*co*-VBC)

A novel carbazole-based monomer 9-(4-vinylbenzyl)-9*H*-carbazole (VBC) was facilely synthesized at room temperature (Scheme S1), and characterized by ^{1}H-nuclear magnetic resonance (^{1}H NMR) spectroscopy, ^{13}C NMR spectroscopy, and high-resolution mass spectrometry (HRMS) (Fig. S1–S3). A series of P(AM-*co*-VBC) with different AM/VBC feed molar ratios of 100 : 1, 200 : 1, 300 : 1, 400 : 1, 500 : 1, and 600 : 1 were synthesized by radical copolymerization of VBC and acrylamide (AM) (Scheme S2), and the relative number-average molecular weight and polydispersity index were determined by gel permeation chromatography (GPC) (Table S1). The photophysical properties of P(AM-*co*-VBC) with an AM/VBC feed molar ratio of 400 : 1 were first investigated using steady-state photoluminescence (PL) and phosphorescence spectra under ambient conditions. The steady-state PL spectrum of P(AM-*co*-VBC) exhibits a major emission peak at 371 nm along with a relatively low peak at 442 nm, whereas the phosphorescence spectrum shows only one distinct emission peak at 442 nm (Fig. 1a). It can be inferred that the emission peak at 371 nm originates from fluorescence, while that at 442 nm corresponds to phosphorescence. Upon varying the excitation wavelength from 220 to 320 nm, the phosphorescence intensity of P(AM-*co*-VBC) at 442 nm reaches a maximum at 245 nm, which is therefore determined as the optimal excitation wavelength (Fig. 1b).

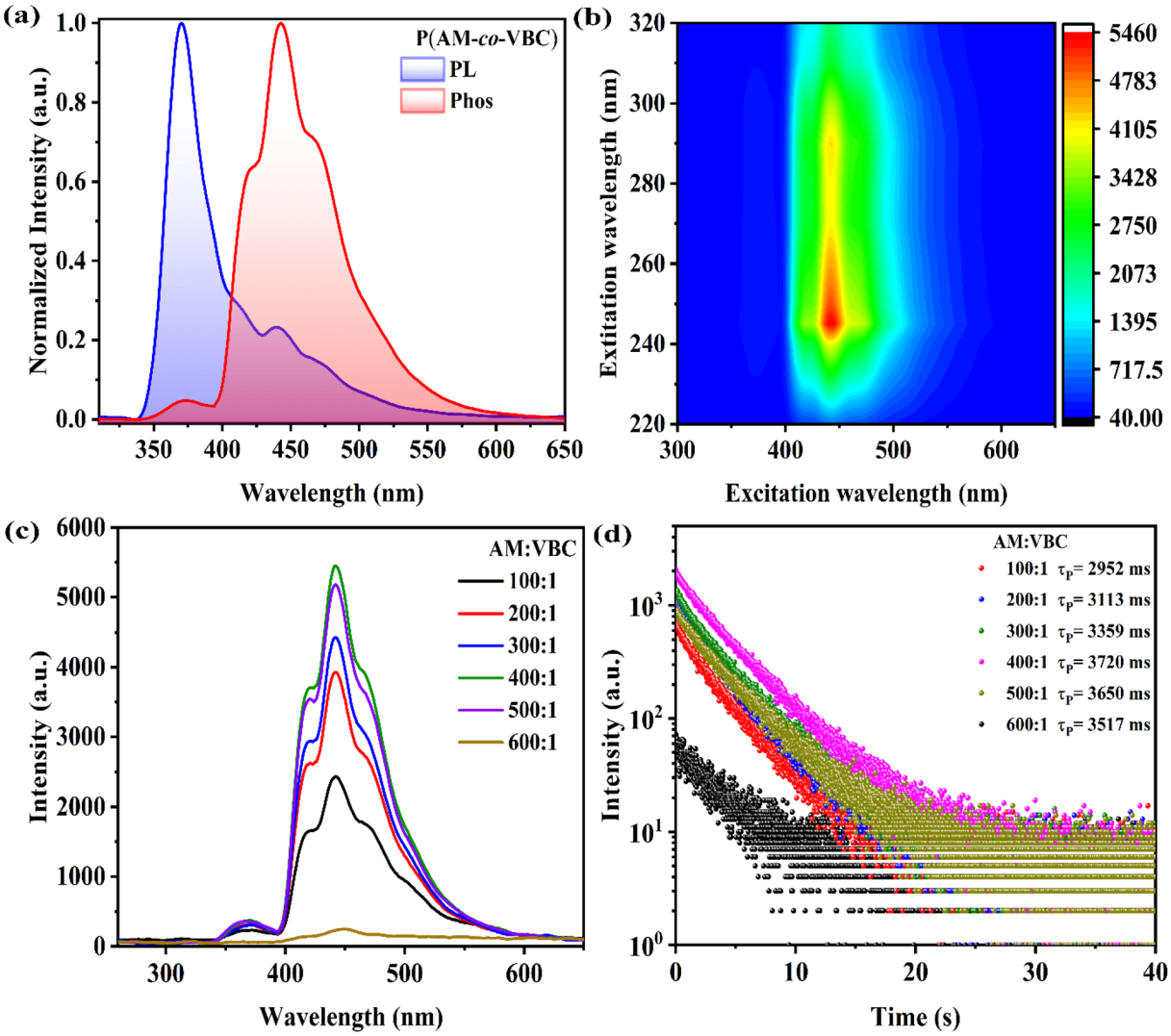

Fig. 1 Photophysical properties of P(AM-*co*-VBC). (a) Steady-state PL and phosphorescence spectra of P(AM-*co*-VBC) with an AM/VBC feed molar ratio of 400 : 1 (λ_{ex} = 245 nm and delay time = 10 ms). (b) Excitation-phosphorescence mapping of P(AM-*co*-VBC) with excitation wavelengths from 220 to 320 nm (delay time = 10 ms). (c) Phosphorescence spectra of P(AM-*co*-VBC) with different AM/VBC feed molar ratios (λ_{ex} = 245 nm and delay time = 10 ms). (d) Time-resolved decay curves of P(AM-*co*-VBC) with different AM/VBC feed molar ratios (λ_{ex} = 245 nm).

Under ambient conditions, pure PAM shows negligible RTP emission with an RTP lifetime of only 2.9 ms (Fig. S4). In contrast, the P(AM-*co*-VBC) copolymers exhibit composition-dependent RTP properties (Fig. 1c and d). Both the phosphorescence intensity and lifetime initially increase with the VBC content, followed by a decrease at higher VBC ratios. P(AM-*co*-VBC) with an AM/VBC feed molar ratio of 400 : 1 has the highest RTP intensity and an exceptionally ultralong RTP lifetime of 3.720 s, accompanied by a considerable RTP quantum yield (QY) of 10.28% (Table S2). After ceasing 254 nm UV light irradiation, P(AM-*co*-VBC) copolymers display bright blue afterglows visible to the naked eye, with the longest lasting 20 s (Fig. S5 and Video S1). Among all synthesized copolymers, P(AM-*co*-VBC) with an AM/VBC feed molar ratio of 400 : 1 presents the best RTP performance (Fig. S6). The excellent RTP properties of P(AM-*co*-VBC) may be attributed to the rigid hydrogen-bonding network between amide groups, which effectively restricts the motion of carbazole groups and thereby suppresses nonradiative decay.[28]

Due to the poor water solubility of the carbazole group, its amphiphilic copolymers can realize the aggregation of carbazole groups through water-induced self-assembly, which triggers aggregation-induced emission enhancement (AIEE).[61] PAM and carbazole are both completely soluble in DMSO. However, P(AM-*co*-VBC) exhibits only weak fluorescence in its DMSO solution, whereas it displays extremely strong fluorescence emission in its aqueous solution (Fig. S7). To investigate its microstructural changes, we conducted dynamic light scattering (DLS) measurements (Fig. S8). In DMSO, a good solvent for both PAM and carbazole, P(AM-*co*-VBC) exhibits a large average hydrodynamic diameter of 601.3 nm, indicating the formation of large, potentially disordered aggregates or entangled networks. This state is unfavorable for radiative transitions of the chromophores, resulting in weak fluorescence. In contrast, in aqueous solution, the DLS spectrum exhibits a main peak with an average diameter of 166.2 nm, accompanied by a minor peak around 9.2 nm. The 166.2 nm nanoparticles clearly confirm the self-assembly of the copolymer in water, forming ordered aggregations with hydrophobic carbazole groups as the core and hydrophilic PAM segments as the shell. The 9.2 nm component likely corresponds to a small fraction of unassembled polymer chains. Within the water-induced aggregations, the hydrophobic carbazole groups are confined within a rigid, restricted microenvironment. This effectively suppresses their non-radiative relaxation pathways, triggering the AIEE effect. The strong fluorescence of P(AM-*co*-VBC) in water originates from its water-induced self-assembly, providing an ideal platform for the AIEE performance of the carbazole chromophore. A dense polymer stacking can effectively suppress luminophore motion, thereby enhancing RTP emission.[62] Therefore, a series of W-P(AM-*co*-VBC) with different AM/VBC feed molar ratios were prepared *via* water dissolution followed by drying, aiming to achieve even better RTP performance. To our excitement, the phosphorescence intensities of W-P(AM-*co*-VBC) obtained from water-dissolution and drying treatment are substantially increased compared to P(AM-*co*-VBC) without water treatment (Fig. 2a and S9). The phosphorescence lifetimes and afterglow durations of W-P(AM-*co*-VBC) are all dramatically extended, with the 400 : 1 AM/VBC ratio sample achieving the longest RTP lifetime of an astonishing 4.664 s and a bright blue afterglow of up to 43 s (Fig. 2b, c and Video S2). Furthermore, the phosphorescence QY of W-P(AM-*co*-VBC) with the AM/VBC feed molar ratio of 400 : 1 is as high as 24.63% (Table S3). The enhancement of the superior RTP properties of W-P(AM-*co*-VBC) may be attributed to the synergy between AIEE from the water-induced self-assembly aggregation of carbazole groups and restriction of molecular motion by the hydrogen-bonding networks in PAM chains. Following water treatment, the glass transition temperature (T_g) of W-P(AM-*co*-VBC) with the AM/VBC feed molar ratio of 400 : 1 increases from 189.4 °C to 215.6 °C (Fig. S10). This rise is likely due to water-induced aggregation of the hydrophobic carbazole groups, which enhances the regular alignment of polymer chains. Consequently, strengthened intermolecular interactions lead to an elevated T_g. Due to the inherently strong hydrophilicity of the PAM segments, W-P(AM-*co*-VBC) undergoes phosphorescence quenching after water vapor exposure. This is attributed to water molecules disrupting the hydrogen bond network between polymer chains, thereby softening its rigid microenvironment. During drying at 120 °C, water molecules are gradually removed with an extended treatment time, leading to a corresponding recovery of RTP performance (Fig. S11). After 25 min of drying, trace water molecules are largely eliminated, allowing RTP strength to recover to its initial level. Based on this mechanism, the material achieves a "water vapor quenching-heat recovery" switching cycle. This RTP switching response can be repeated at least six times, demonstrating excellent reversibility. The recovery efficiency of the RTP intensity exhibits a gradual decline with repeated cycles. This attenuation is likely due to trace water molecules remaining within the system in the form of bound water, which cannot be completely removed under short-duration heating. The presence of these trace water molecules disrupts the hydrogen-bonding network among the PAM chains, thereby impeding the re-establishment of a rigid microenvironment essential for suppressing non-radiative decay and, consequently, the full recovery of phosphorescence.[63]

To investigate the influence of polymer matrices on RTP performance, we synthesized three copolymers with distinct matrices: P(VA-*co*-VBC), P(VP-*co*-VBC), and P(MMA-*co*-VBC). Only P(VA-*co*-VBC) exhibits a distinct afterglow of 1 s upon removal of 254 nm UV irradiation, whereas P(VP-*co*-VBC) and P(MMA-*co*-VBC) show no significant afterglow (Fig. S12). After water treatment of P(VA-*co*-VBC) and P(VP-*co*-VBC), the afterglow duration of W-P(VA-*co*-VBC) is remarkably extended to 10 s, while W-P(VP-*co*-VBC) still displays no afterglow. Considering that PVA chains are rich in hydroxyl groups capable of forming dense intermolecular hydrogen bond networks, water treatment may further optimize this network, resulting in strong and ordered hydrogen-bonding interactions. Although PVP can also participate in hydrogen bonding, its molecular structure may not support the formation of a similarly rigid and protective network. PMMA lacks strong hydrogen-bonding capability altogether. Therefore, the significant enhancement

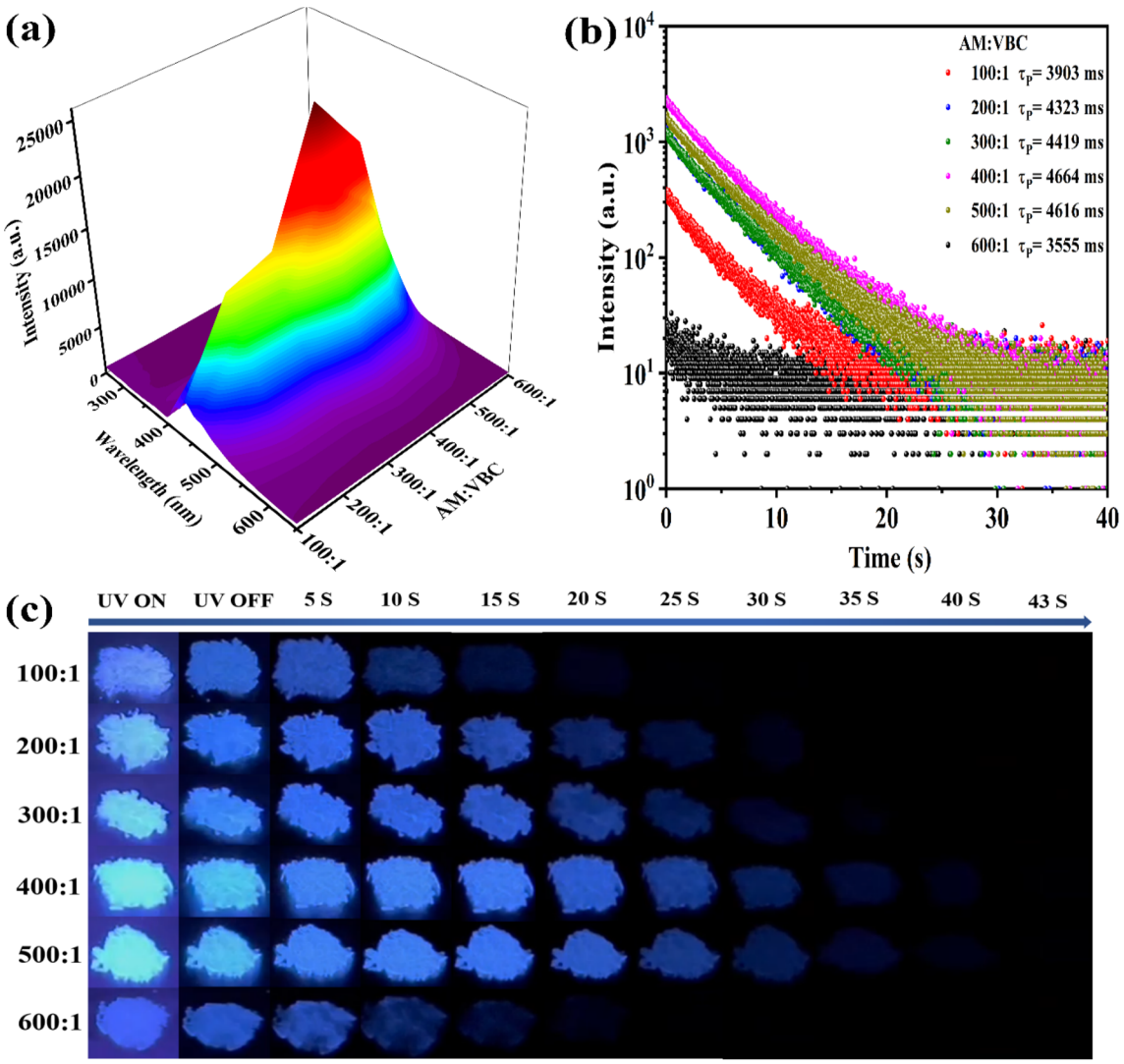

Fig. 2 Photophysical properties of W-P(AM-*co*-VBC). (a) Phosphorescence spectra of W-P(AM-*co*-VBC) with different AM/VBC feed molar ratios (λ_{ex} = 245 nm and delay time = 10 ms). (b) Time-resolved decay curves of W-P(AM-*co*-VBC) with different AM/VBC feed molar ratios (λ_{ex} = 245 nm). (c) Photographs of W-P(AM-*co*-VBC) under 254 nm UV light and after ceasing the irradiation.

of afterglow in W-P(VA-*co*-VBC) also demonstrates that the synergistic effect of water treatment-triggered hydrogen bond network strengthening and AIEE contributes to the superior RTP performance.

Theoretical calculation

To deeply understand the excellent RTP performance of P(AM-*co*-VBC), theoretical calculations were performed using isolated 9-benzyl-9*H*-carbazole (BC) and BC dimer as models. In the isolated BC, the highest occupied molecular orbital (HOMO) and lowest unoccupied molecular orbital (LUMO) electron densities are localized on the carbazole group (Fig. 3a). As shown in Fig. 3b and c, the electron clouds of the HOMO and LUMO are distributed over two molecules in the systems of BC dimer, and apparent charge transfer (CT) from one carbazole group to another is observed. The electron cloud aggregation on the carbazole group and the intermolecular CT both favor the occurrence of intersystem crossing (ISC) to facilitate RTP emission. The formation of the molecular dimer is conducive to the generation of intermolecular CT, which also promotes the exciton transition from the excited singlet state to the triplet state.[64] The HOMO–LUMO energy gaps of two BC dimers are all reduced compared to the isolated BC. Smaller ΔE_{ST} (<0.37 eV) and larger SOC constants (>0.3 cm^{-1}) are favorable for promoting the ISC process to achieve phosphorescence emission.[65] Time-dependent density functional theory (TD-DFT) is applied to calculate ΔE_{ST} and SOC constants of isolated BC and BC dimers (Fig. 3d–f and Table S4). Isolated BC and two BC dimers all contain multiple triplet states with ΔE_{ST} values below 0.37 eV. However, isolated BC has no effective ISC channels satisfying $\xi(S_1–T_n)$ > 0.3 cm^{-1}, while the two BC dimers both have four effective ISC channels. The presence of effective ISC channels suggests that BC dimers help to promote ISC and thus extend the phosphorescence lifetime. Meanwhile, the T_1 states of the BC dimers exhibit a high degree of (π, π^*) configuration characteristics, and therefore the decay rate is relatively slow

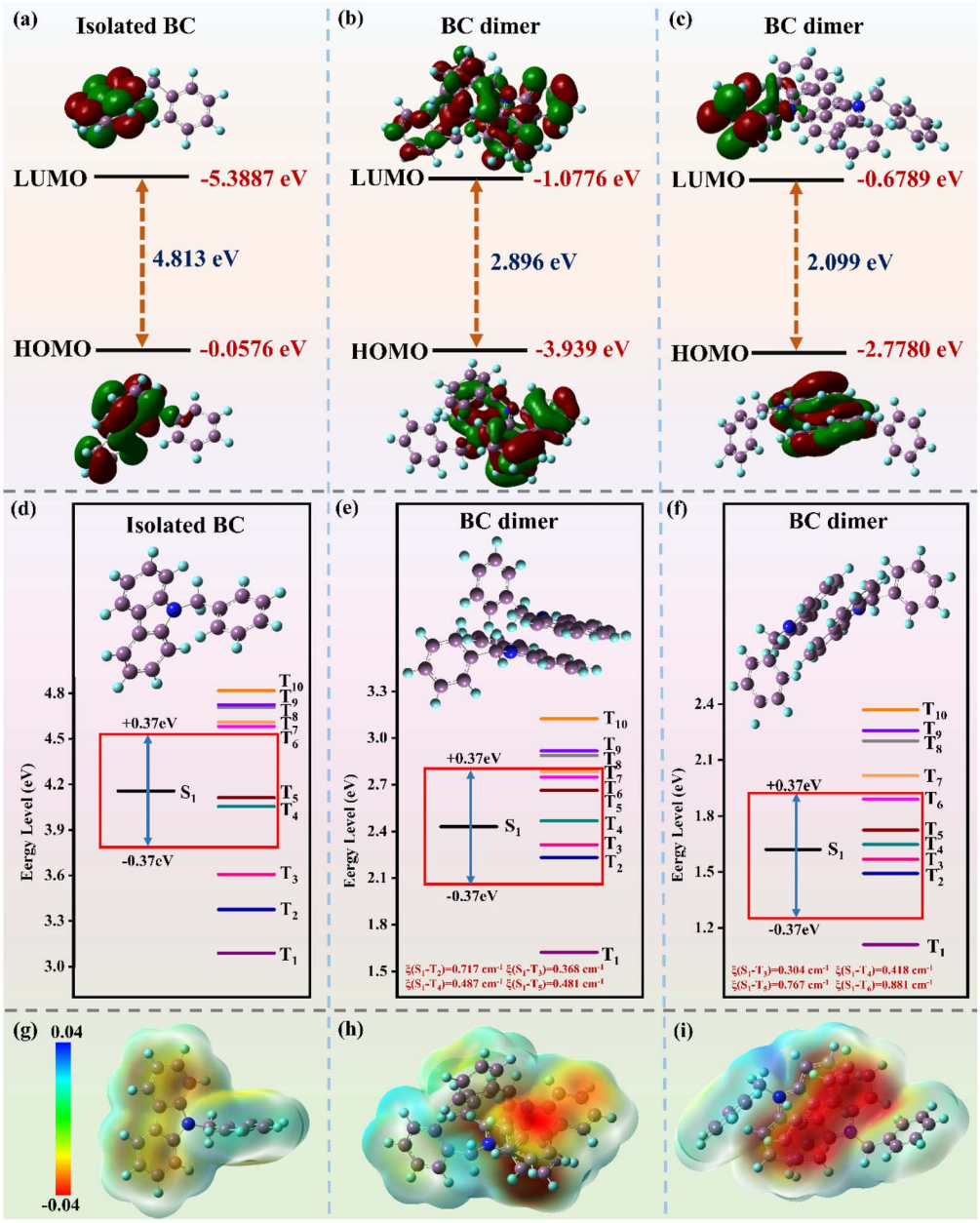

Fig. 3 Theoretical calculation of the isolated BC and BC dimer. The highest occupied molecular orbital (HOMO) and lowest unoccupied molecular orbital (LUMO) energy levels of (a) isolated BC and (b and c) BC dimer. The energy levels of (d) isolated BC and (e and f) BC dimer. The calculated electrostatic potential (ESP) maps of (g) isolated BC and (h and i) BC dimer.

(Tables S5–S7). The rigid environment, stabilized by stronger (π, π^*) interaction between BC molecules and enhanced intermolecular interactions, leads to a significantly faster ISC rate and a slower phosphorescence decay rate, thereby improving RTP performance.[66,67] As illustrated in Fig. 3g–i, the isolated BC and BC dimers all present a dense electron density (the red region) on the carbazole group, while other parts show a lower electron density, further indicating the presence of CT in the excited state of the isolated BC and BC dimers. The intermolecular CT between the dimers contributes to the lowering of the energy gaps, thereby promoting the ISC process.[68] The results indicate that aggregation facilitates ISC to realize RTP emission, further demonstrating that the aggregation of carbazole groups plays a significant role in the superior RTP performance of W-P(AM-*co*-VBC).

Color-tunable afterglow through phosphorescence FRET

Benefiting from its broad phosphorescence emission spanning from 400 to 600 nm and ultralong RTP lifetime, W-P(AM-*co*-VBC) with the AM/VBC feed molar ratio of 400 : 1 has potential as an energy donor for developing color-tunable long afterglow materials through the phosphorescence FRET strategy. As shown in Fig. 4a, the UV-vis absorption spectra of the commercially available fluorescent dyes calcein (CAL),

fluorescein (FL), rhodamine 6G (R6G), and sulforhodamine B (SRB) exhibit significant overlap with the RTP emission band of W-P(AM-*co*-VBC), nicely fulfilling the prerequisite for the phosphorescence FRET. Therefore, we construct a series of ternary doping systems using W-P(AM-*co*-VBC) as the energy donor and CAL, FL, R6G, and SRB as the acceptors, aiming to achieve color-tunable long afterglows *via* phosphorescence FRET (Fig. 4b).

The phosphorescence FRET of the CAL doped system W-P(AM-*co*-VBC)/CAL is first studied. In contrast to PAM/CAL with no observable RTP emission peaks, the phosphorescence spectrum of W-P(AM-*co*-VBC)/CAL exhibits two delayed emission peaks at 442 and 554 nm (Fig. S13). The steady-state PL spectrum of PAM/CAL displays a single peak at 554 nm, which overlaps well with the phosphorescence peak of W-P(AM-*co*-VBC)/CAL. It can be inferred that the phosphorescence FRET occurs in the W-P(AM-*co*-VBC)/CAL system with the 442 nm peak belonging to the phosphorescence of the energy donor W-P(AM-*co*-VBC) and the 554 nm peak originating from the delayed fluorescence of the energy acceptor CAL. As can be seen from Fig. 4c, the intensity of the 442 nm emission peak gradually decreases with increasing CAL doping ratio, while the delayed fluorescence emission peaks originating from CAL show a tendency of first enhancement and then decrease, accompanied by an obvious red-shift. At higher CAL doping ratios, the decrease in intensity and red-shift of the CAL emission peaks may be attributed to the aggregation of excess CAL.[69] Meanwhile, the RTP lifetime at 442 nm decreases monotonically with increasing CAL doping ratio, and the longest lifetime of the delayed fluorescence from CAL reaches up to 3.837 s (Fig. 4d and e). As the CAL doping ratio increases from 0.11 to 1.98, both the delayed fluorescence QY and the energy transfer efficiency show significant enhancement, increasing from 12.60% to 29.63% and from 12.01% to 32.80%, respectively (Table S8). More interestingly, the afterglow color can be tuned from cyan to yellow-green by precisely adjusting the CAL

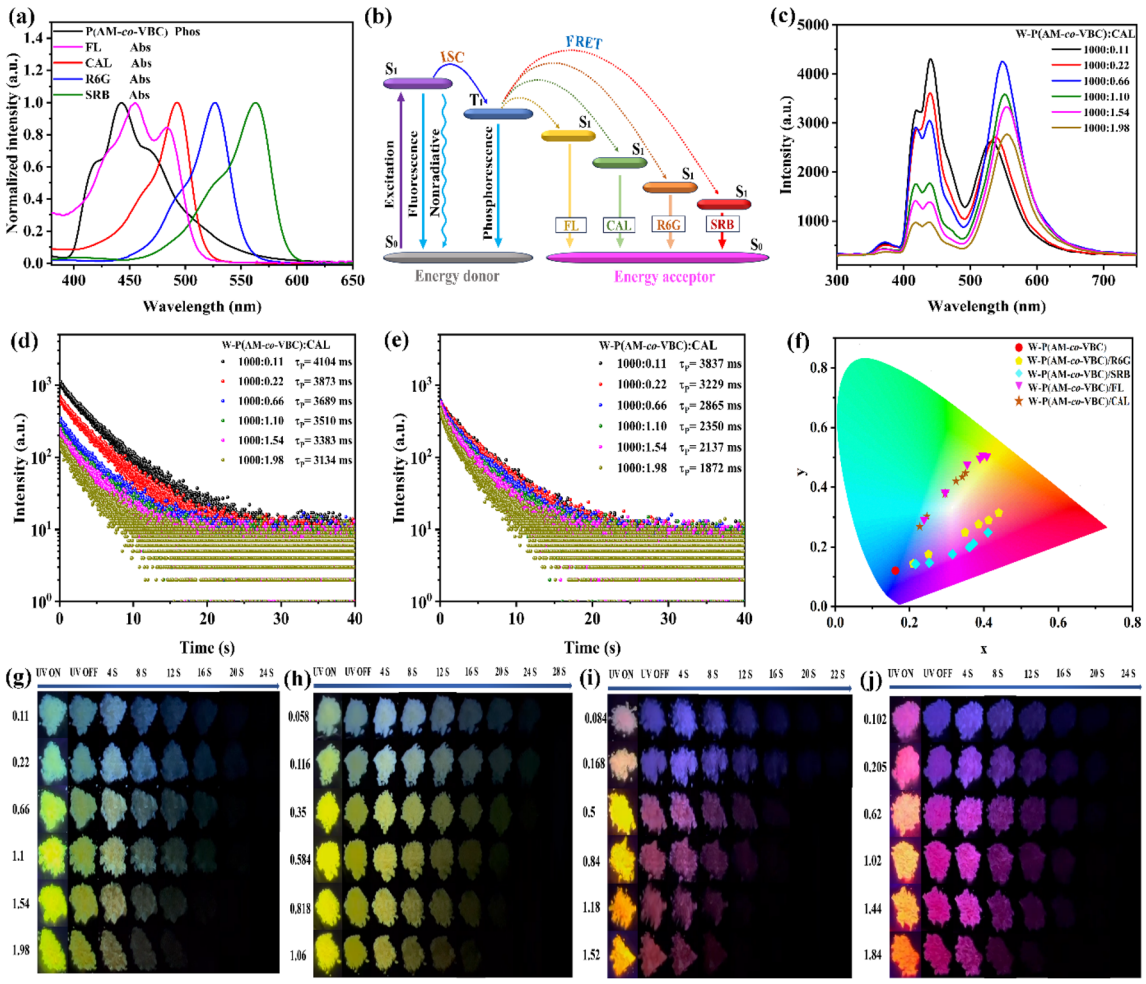

Fig. 4 Color-tunable afterglow through phosphorescence FRET. (a) Phosphorescence spectrum of W-P(AM-*co*-VBC) with an AM/VBC feed molar ratio of 400 : 1 and UV-vis absorption spectra of FL, CAL, R6G and SRB. (b) Simplified Jablonski diagram to illustrate the phosphorescence FRET process. (c) Phosphorescence spectra of W-P(AM-*co*-VBC)/CAL with different weight ratios (λ_{ex} = 245 nm and delayed time = 10 ms). Time-resolved decay curves of W-P(AM-*co*-VBC)/CAL at 442 nm (d) and 554 nm (e) (λ_{ex} = 245 nm). (f) CIE chromaticity diagram corresponding to the phosphorescence spectra of W-P(AM-*co*-VBC), W-P(AM-*co*-VBC)/CAL, W-P(AM-*co*-VBC)/FL, W-P(AM-*co*-VBC)/R6G and W-P(AM-*co*-VBC)/SRB with different weight ratios. Photographs of W-P(AM-*co*-VBC)/CAL (g), W-P(AM-*co*-VBC)/FL (h), W-P(AM-*co*-VBC)/R6G (i) and W-P(AM-*co*-VBC)/SRB (j) under 254 nm UV light irradiation and after ceasing the irradiation.

doping content (Fig. 4g and Video S3). The change of the long afterglow color is also further demonstrated by the progressive shift in Commission Internationale de l'Eclairage (CIE) coordinates (Fig. 4f). The results unambiguously indicate efficient phosphorescence FRET in the W-P(AM-*co*-VBC)/CAL system, enabling good afterglow color tunability.

Subsequently, a series of doping systems W-P(AM-*co*-VBC)/FL, W-P(AM-*co*-VBC)/R6G, and W-P(AM-*co*-VBC)/SRB were prepared to study phosphorescence FRET in the case of different energy acceptors. Similar to the W-P(AM-*co*-VBC)/CAL system, except for the phosphorescence peak originating from P(AM-*co*-VBC), the phosphorescence spectra of W-P(AM-*co*-VBC)/FL, W-P(AM-*co*-VBC)/R6G and W-P(AM-*co*-VBC)/SRB all exhibit a strong emission peak in the 500–700 nm range, which can overlap with the fluorescence peaks of PAM/FL, PAM/R6G and PAM/SRB, respectively (Fig. S14–S16). The RTP spectra of PAM/FL, PAM/R6G and PAM/SRB do not show any obvious emission peaks in the 500–700 nm range under ambient conditions. The emission peaks at 548, 590 and 618 nm in the RTP spectra of W-P(AM-*co*-VBC)/FL, W-P(AM-*co*-VBC)/R6G, and W-P(AM-*co*-VBC)/SRB are attributed to the delayed fluorescence of FL, R6G and SRB, respectively. Therefore, it can be concluded that the prepared W-P(AM-*co*-VBC)/FL, W-P(AM-*co*-VBC)/R6G, and W-P(AM-*co*-VBC)/SRB systems are all capable of achieving delayed long-wavelength fluorescence emission *via* phosphorescence FRET. As shown in Fig. S17, the phosphorescence emission intensity from W-P(AM-*co*-VBC) in all three doping systems decreases progressively with increasing doping amount of small-molecule fluorescent dyes, while the delayed fluorescence intensity from small-molecule fluorescent dyes all initially increases and then declines, accompanied by a red-shift of the emission peaks. Due to the occurrence of phosphorescence FRET, the phosphorescence lifetime of W-P(AM-*co*-VBC) in all three systems decreases with increasing fluorescent dye doping content, and the longest delayed fluorescence lifetimes can reach up to 3.731 s for FL, 3.655 s for R6G, and 2.864 s for SRB (Fig. S18–S20). The delay fluorescence QYs can surprisingly reach 55.22%, 32.76%, and 46.72% when the doping weight ratios of FL, R6G, and SRB are 1.06, 1.18, and 1.84, respectively (Tables S9–S11). In all three systems, the energy transfer efficiency also increases progressively with the rise in fluorescent dye loading, confirming

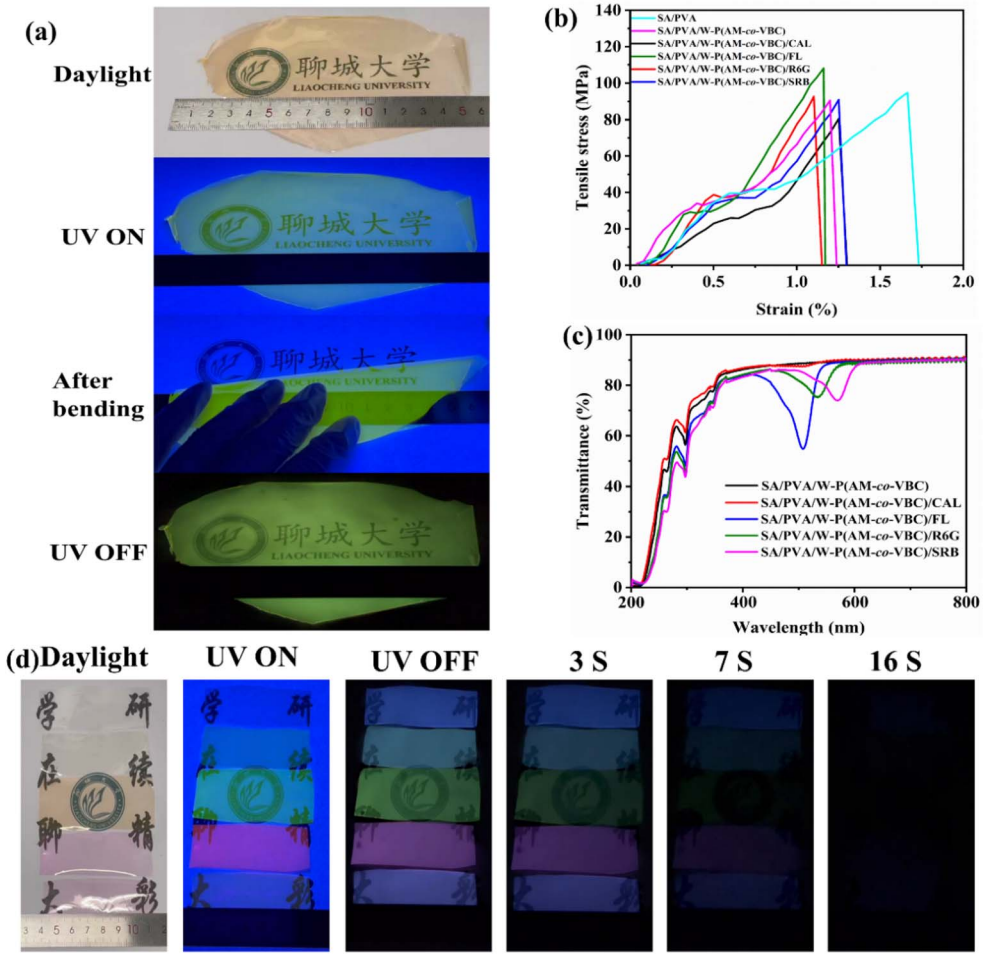

Fig. 5 Properties of flexible multicolor RTP films. (a) Photographs of the flexible SA/PVA/W-P(AM-*co*-VBC)/FL film under daylight, 254 nm UV light irradiation and after ceasing the irradiation. (b) Stress–strain curves of SA-based flexible films. (c) Transmittance performance of SA/PVA/W-P(AM-*co*-VBC), SA/PVA/W-P(AM-*co*-VBC)/CAL, SA/PVA/W-P(AM-*co*-VBC)/FL, SA/PVA/W-P(AM-*co*-VBC)/R6G and SA/PVA/W-P(AM-*co*-VBC)/SRB films. (d) Transparency performance of flexible multicolor RTP films under daylight, 254 nm UV light irradiation and after ceasing the irradiation.

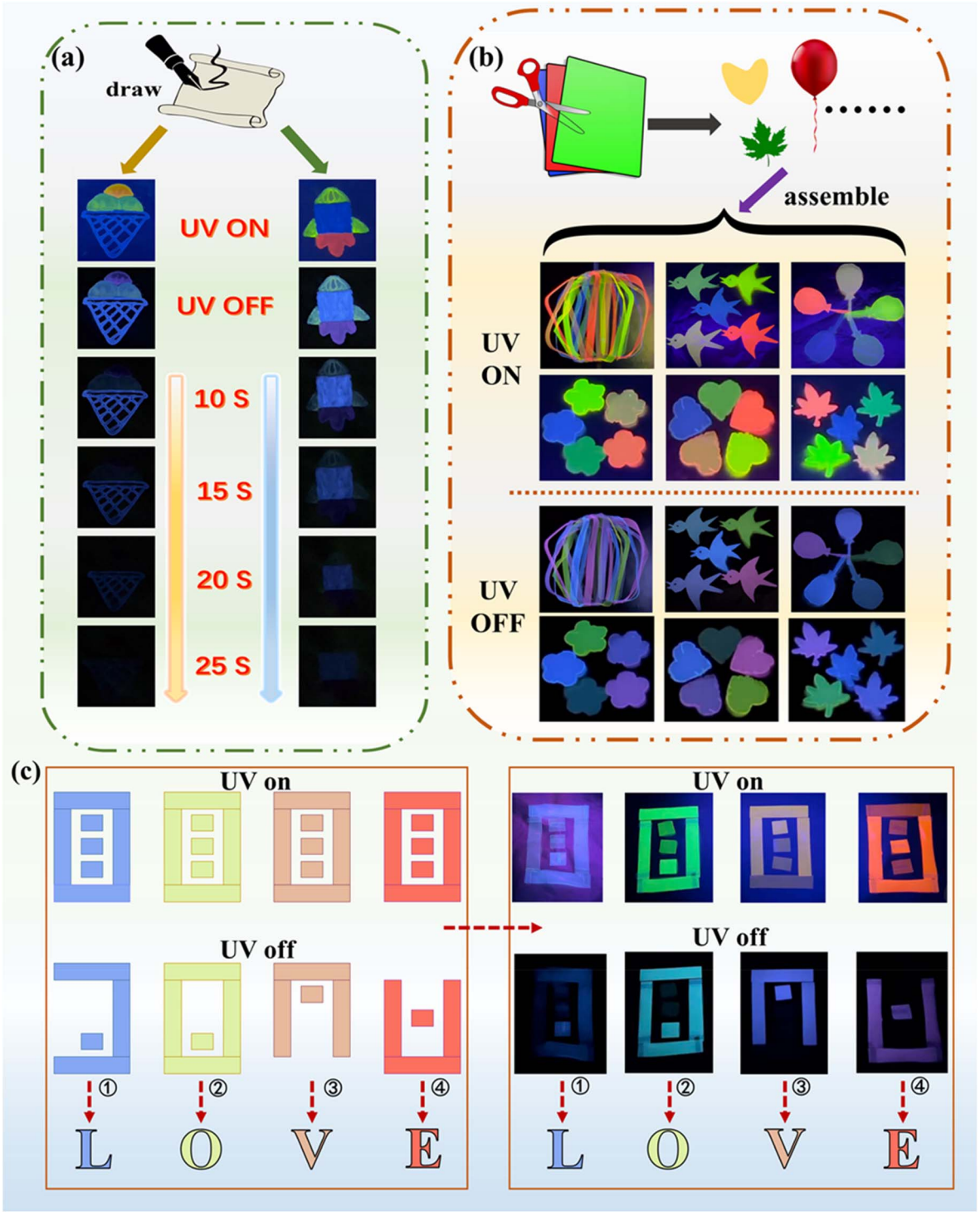

Fig. 6 Applications of multicolor RTP materials. (a) Colorful patterns composed of different RTP materials under 254 nm UV light irradiation and after ceasing the irradiation. (b) Flexible multicolor RTP films with different shapes under 254 nm UV light irradiation and after ceasing the irradiation. (c) Information encryption applications of multicolor flexible RTP films.

the successful FRET from the phosphorescent donor. Furthermore, by adjusting the doping content of small-molecule fluorescent dyes, all three doping systems exhibit multicolor afterglow tunability, achieving long afterglow color transitions from cyan to yellow, from blue to rosy red, and from blue to purple, respectively, under ambient conditions (Fig. 4f, h–j and Videos S4–S6). The above results demonstrate the feasibility of conveniently constructing high-performance multicolor RTP materials through the phosphorescence FRET strategy using W-P(AM-*co*-VBC) as

a universal energy donor and commercial fluorescent dyes as energy acceptors.

Properties of flexible multicolor RTP films

As a natural polysaccharide extracted from algal organisms, sodium alginate (SA) has the advantage of being widely available and biocompatible, and its use aligns with green and sustainable development. We have previously realized the transformation of SA films from brittle to flexible by the modulation of trace polyhydroxy compounds.[57] Therefore, SA as the matrix and trace PVA as the regulator were used to explore the construction of flexible long-lifetime multicolor RTP films. As shown in Fig. 5a and S21, large-area multicolor RTP films from SA/PVA/W-P(AM-*co*-VBC), SA/PVA/W-P(AM-*co*-VBC)/CAL, SA/PVA/W-P(AM-*co*-VBC)/FL, SA/PVA/W-P(AM-*co*-VBC)/R6G, and SA/PVA/W-P(AM-*co*-VBC)/SRB are prepared by a convenient doping-coating-drying process. All films exhibit excellent flexibility and can be bent repeatedly without damage. To evaluate their mechanical robustness for practical applications, the tensile properties of the flexible multicolor RTP films with about 20 μm thickness are tested at a stretching rate of 20 mm min^{-1} under ambient conditions (Fig. 5b). To our excitement, the fracture strengths of the prepared films all exceed 80 MPa, with the SA/PVA/W-P(AM-*co*-VBC)/FL film achieving the highest value of 110 MPa. Compared with the longer elongation at break of SA/PVA, the elongation at break of the flexible multicolor film prepared by doping with RTP materials decrease to a certain extent, which may be attributed to the increased brittleness from the incorporation of the rigid multicolor RTP materials. The tensile stresses of the prepared SA-based flexible RTP films are higher than those of many previously reported polymer-based RTP films, indicating their superior mechanical strength (Fig. S22). The high transmittance of the flexible multicolor RTP films in the visible region confirms their excellent transparency (Fig. 5c). The transparency of the prepared flexible multicolor RTP films is further demonstrated through observation under daylight and 254 nm UV light as well as afterglow display, and the multicolor afterglows can last for up to 16 s (Fig. 5d and Video S7). Amazingly, the prepared flexible multicolor RTP films all have ultralong phosphorescence lifetimes of more than 1 s, reaching 4.215, 2.655, 1.905, 1.960, and 2.273 s for SA/PVA/W-P(AM-*co*-VBC), SA/PVA/W-P(AM-*co*-VBC)/CAL, SA/PVA/W-P(AM-*co*-VBC)/FL, SA/PVA/W-P(AM-*co*-VBC)/R6G, and SA/PVA/W-P(AM-*co*-VBC)/SRB, respectively (Fig. S23). The prepared SA-based flexible RTP films exhibit superior phosphorescence lifetime and QY compared to most reported polymer-based RTP films (Fig. S24). The surface morphology of the flexible RTP films was characterized by FESEM (Fig. S25). While pits are present due to water evaporation during drying, their distribution is homogeneous throughout all films. This uniform microstructure underlies the consistent performance of the flexible RTP films. Additionally, the effects of ambient temperature, humidity, and tensile stress on the phosphorescence properties of the prepared films were investigated. Although phosphorescence typically undergoes thermal quenching in all flexible films, the SA/PVA/W-P(AM-*co*-VBC) film retains an ultralong phosphorescence lifetime of 380 ms even at an elevated temperature of 393 K (Fig. S26–S30). Despite the hydrophilic nature of their components, the phosphorescence properties of the flexible films show only a slight, humidity-dependent decrease after 10 min exposure even at a high relative humidity of 80%, demonstrating moderate moisture resistance (Fig. S31–S35). Even when subjected to a tensile force of approximately 5 N, the flexible films continue to exhibit a bright and long afterglow, confirming their mechanical robustness for practical applications (Fig. S36).

Applications of polymer-based RTP materials

Based on the exceptional properties of the prepared long-lifetime multicolor RTP materials, their potential applications in advanced information encryption and multiple flexible display are demonstrated. We first attempted advanced information encryption by drawing patterns on paper using the multicolored RTP material as ink. As shown in Fig. 6a, an ice cream pattern is designed by coating the ice cream bucket with P(AM-*co*-VBC), two ice cream balls at the bottom with P(AM-*co*-VBC)/CAL, and the top ball with P(AM-*co*-VBC)/R6G. A clear multicolor ice cream pattern is observed under 254 nm UV light. After turning off the UV light, the top ice cream ball disappears within 10 s, while only the bucket's afterglow persists for more than 20 s, thereby revealing an encrypted pattern (Video S8). Meanwhile, a rocket pattern is drawn by using P(AM-*co*-VBC) for the rocket body, P(AM-*co*-VBC)/FL for the rocket head and wings, and P(AM-*co*-VBC)/SRB for the flame. After turning off the UV light, the bright multicolor rocket pattern gradually becomes incomplete. As time progresses, the red flame fades first, followed by the yellow-green rocket head and wings, and only the blue rocket body pattern, which is encrypted, remains visible for over 20 s (Video S9). Furthermore, with a view to being used for multicolor displays, flexible ribbons cut out from the large-area flexible multicolor RTP films are assembled into a colorful lantern that displays bright multicolor afterglows when the 254 nm UV light is turned off (Fig. 6b and Video S10). In addition, the prepared large-area flexible multicolor RTP films can be conveniently tailored into diverse shapes with different colors as needed, such as birds, balloons, flower petals, hearts, and leaves, which all display bright colored long afterglows under ambient conditions (Videos S11–S15). Fig. 6c demonstrates information encryption using multicolor RTP films. Under 254 nm UV light, the films show four identically shaped patches emitting different colors. After turning off the UV light, each patch reveals a distinct phosphorescent pattern. According to the Masonic code, these patterns correspond to the letters "L" (for pattern ①), "O" (②), "V" (③), and "E" (④). Thus, the decrypted message "LOVE" is disclosed solely by the afterglow, showcasing a high-level of information concealment.

Conclusions

In summary, we have successfully synthesized bright blue PAM-based ultralong RTP materials P(AM-*co*-VBC) by radical binary copolymerization. After water-dissolution and drying treatment,

the bright blue long afterglow of W-P(AM-*co*-VBC) extends from 20 to 43 s due to the AIEE effect arising from the self-assembly aggregation of carbazole groups. The ultralong RTP lifetime of W-P(AM-*co*-VBC) reaches an astonishing 4.664 s with the phosphorescence QY of up to 24.63%. In addition, the phosphorescence FRET strategy is employed to facilely construct multicolor ultralong RTP materials, using W-P(AM-*co*-VBC) as an energy donor and commercially available fluorescent dyes FL, CAL, R6G, and SRB as energy acceptors. Amazingly, the constructed multicolor RTP materials show color-tunable persistent afterglow from cyan to yellow, pink, and purple with second-scale RTP lifetimes of 3.837, 2.416, 2.452, and 1.993 s, respectively. Using a simple doping-coating-drying process, flexible multicolor ultralong RTP films are fabricated over large areas by doping multicolor RTP materials into SA matrices with trace amounts of PVA as a regulator. Interestingly, the prepared multicolor RTP films with phosphorescence lifetimes of more than 1 s exhibit excellent flexibility and high transparency. The extraordinary properties make the prepared multicolor ultralong RTP materials and flexible films promising for advanced information encryption and multiple flexible display. This work not only provides guidelines for developing multicolor RTP materials with second-scale phosphorescence lifetimes and convenient large-area preparation of flexible multicolor RTP films, but also expands flexible multicolor RTP materials to natural polymers.

Author contributions

G. L. conceived and designed the experiments. F. R. T. and G. L. guided the process. T. Y. L. and Y. Z. carried out all the experiments and characterization. S. C. S., Y. T. Z., Z. H. W., F. L., and L. P. W. analyzed the data. All authors discussed the results and contributed to preparing the manuscript.

Conflicts of interest

There are no conflicts to declare.

Data availability

The data that support the findings of this study are available from the corresponding author upon reasonable request.

Supplementary information (SI): materials and measurements, experimental details, spectral data and additional data. See DOI: https://doi.org/10.1039/d6sc00779a.

Acknowledgements

This work was supported by the National Natural Science Foundation of China (Grant No. 51503094), Natural Science Foundation of Shandong Province (Grant No. ZR2021ME149 and ZR2021ME126), and Research Foundation of Liaocheng University (Grant No. 318011905).

Notes and references

1 F. Li, M. Wang, S. Liu and Q. Zhao, *Chem. Sci.*, 2022, **13**, 2184.
2 W. Qin, J. Ma, Y. Zhou, Q. Hu, Y. Zhou and G. Liang, *Chem. Eng. J.*, 2020, **400**, 125934.
3 C. Si, T. Wang, A. Gupta, D. Cordes, A. Slawin, J. Siegel and E. Zysman-Colman, *Angew. Chem., Int. Ed.*, 2023, **62**, e202309718.
4 H. Ding, Y. Sun, M. Tang, g. Wen, S. Yue, Y. Peng, F. Li, L. Zheng, S. Wang, Y. Shi and Q. Cao, *Chem. Sci.*, 2023, **14**, 4633–4640.
5 Y. Su, S. Phua, Y. Li, X. Zhou, D. Jana, G. Liu, W. Lim, W. Ong, C. Yang and Y. Zhao, *Sci. Adv.*, 2018, **4**, eaas9732.
6 P. She, J. Lu, Y. Qin, F. Li, J. Wei, Y. Ma, W. Wang, S. Liu, W. Huang and Q. Zhao, *Cell Rep. Phys. Sci.*, 2021, **2**, 100505.
7 K. Zhang, Q. Yu, H. Wei, S. Liu, Q. Zhao and W. Huang, *Chem. Rev.*, 2018, **118**, 1770–1839.
8 J. Zhi, Q. Zhou, H. Shi, Z. An and W. Huang, *Chem.–Asian J.*, 2020, **15**, 947–957.
9 Y. Zhang, L. Hairong, M. Yang, W. Dai, J. Shi, B. Tong, Z. Cai, Z. Wang, Y. Dong and X. Yu, *Chem. Commun.*, 2023, **59**, 5329–5342.
10 G. Zhan, Z. Liu, Z. Bian and C. Huang, *Front. Chem.*, 2019, **7**, 305.
11 Z. Zhou, X. Xie, Z. Sun, X. Wang, Z. An and W. Huang, *J. Mater. Chem. C*, 2023, **11**, 3143–3161.
12 T. Zhang, X. Ma, H. Wu, L. Zhu, Y. Zhao and H. Tian, *Angew. Chem., Int. Ed.*, 2020, **59**, 11206–11216.
13 Z. Xu, Y. He, H. Shi and Z. An, *SmartMat*, 2023, **4**, e1139.
14 R. Tian, S. Xu, Q. Xu and C. Lu, *Sci. Adv.*, 2020, **6**, eaaz6107.
15 X. Liu, L. Yang, X. Li, L. Zhao, S. Wang, Z. Lu, J. Ding and L. Wang, *Angew. Chem., Int. Ed.*, 2021, **60**, 2455–2463.
16 Y. Gong, J. Yang, M. Fang and Z. Li, *Cell Rep. Phys. Sci.*, 2022, **3**, 100663.
17 L. Gao, Y. Zhang, X. Chen, Y. Zheng, X. Zheng, C. Wang, Z. Wang, J. Hao, Q. Tian, X. Yu, C. Yang, Y. Li and Y. Zhao, *Adv. Opt. Mater.*, 2021, **9**, 2101284.
18 Y. Gao, Z. Deng, F. Wang and P. Sun, *Mater. Chem. Front.*, 2022, **6**, 1068–1078.
19 J. Guo, C. Yang and Y. Zhao, *Acc. Chem. Res.*, 2022, **55**, 1160–1170.
20 R. Liu, B. Ding, D. Liu and X. Ma, *Chem. Eng. J.*, 2021, **421**, 129732.
21 Y. Xu, Y. Zhu, L. Kong, S. Sun, F. Li, F. Tao, L. Wang and G. Li, *Chem. Eng. J.*, 2023, **453**, 139753.
22 G. Zhang, J. Chen, S. Payne, S. Kooi, J. Demas and C. Fraser, *J. Am. Chem. Soc.*, 2007, **129**, 8942–8943.
23 W. Zhu, H. Xing, E. Li, H. Zhu and F. Huang, *Macromolecules*, 2022, **55**, 9802–9809.
24 X. Lin, C. Xu, Y. Qiu and X. Ma, *Ind. Eng. Chem. Res.*, 2023, **62**, 13053–13060.
25 X. Zhang, C. Qian, Z. Ma, X. Fu, Z. Li, H. Jin, M. Chen, H. Jiang and Z. Ma, *Adv. Sci.*, 2023, **10**, 2206482.
26 C. Wang, L. Qu, X. Chen, Q. Zhou, Y. Yang, Y. Zheng, X. Zheng, L. Gao, J. Hao, L. Zhu, B. Pi and C. Yang, *Adv. Mater.*, 2022, **34**, 2204415.

27 C. Qian, Z. Ma, X. Fu, X. Zhang, Z. Li, H. Jin, M. Chen, H. Jiang, X. Jia and Z. Ma, *Adv. Mater.*, 2022, **34**, 2200544.
28 D. Wang, H. Wu, J. Gong, Y. Xiong, Q. Wu, Z. Zhao, L. Wang, D. Wang and B. Tang, *Mater. Horiz.*, 2022, **9**, 1081–1088.
29 D. Li, Y. Yang, J. Yang, M. Fang, B. Tang and Z. Li, *Nat. Commun.*, 2022, **13**, 347.
30 S. Xiong, Y. Xiong, D. Wang, Y. Pan, K. Chen, Z. Zhao, D. Wang and B. Tang, *Adv. Mater.*, 2023, **35**, 2301874.
31 L. Kong, Y. Zhu, S. Sun, H. Li, F. Tao, F. Li, L. Wang and G. Li, *J. Mater. Chem. C*, 2023, **11**, 1960–1970.
32 L. Kong, Y. Zhu, S. Sun, H. Li, S. Dong, F. Li, F. Tao, L. Wang and G. Li, *Chem. Eng. J.*, 2023, **469**, 143931.
33 Q. Chen, L. Qu, H. Hou, J. Huang, C. Li, Y. Zhu, Y. Wang, X. Chen, Q. Zhou, Y. Yang and C. Yang, *Nat. Commun.*, 2024, **15**, 2947.
34 N. Gan, H. Shi, Z. An and W. Huang, *Adv. Funct. Mater.*, 2018, **28**, 1802657.
35 M. Kwon, D. Lee, S. Seo, J. Jung and J. Kim, *Angew. Chem., Int. Ed.*, 2014, **53**, 11177–11181.
36 J. Xu, A. Takai, Y. Kobayashi and M. Takeuchi, *Chem. Commun.*, 2013, **49**, 8447–8449.
37 X. Chen, C. Xu, T. Wang, C. Zhou, J. Du, Z. Wang, H. Xu, T. Xie, G. Bi, J. Jiang, X. Zhang, J. Demas, C. Trindle, Y. Luo and G. Zhang, *Angew. Chem., Int. Ed.*, 2016, **55**, 9872–9876.
38 H. Chen, X. Yao, X. Ma and H. Tian, *Adv. Opt. Mater.*, 2016, **4**, 1397–1401.
39 J. Liu, G. Liu, S. Zhang, S. Xue, Q. Sun and W. Yang, *ACS Mater. Lett.*, 2025, **7**, 876–883.
40 H. Ma, Y. Qin, N. Zhang, H. Mu, J. Liu, S. Xue, Q. Sun and W. Yang, *Adv. Mater.*, 2025, **37**, 2510443.
41 R. Deng, F. Qin, R. Chen, W. Huang, M. Hong and X. Liu, *Nat. Nanotechnol.*, 2015, **10**, 237–242.
42 J. Lee, P. Bisso, R. Srinivas, J. Kim, A. Swiston and P. Doyle, *Nat. Mater.*, 2014, **13**, 524–529.
43 L. Pan, S. Sun, A. Zhang, K. Jiang, L. Zhang, C. Dong, Q. Huang, A. Wu and H. Lin, *Adv. Mater.*, 2015, **27**, 7782–7787.
44 Y. Lei, W. Dai, J. Guan, S. Guo, F. Ren, Y. Zhou, J. Shi, B. Tong, Z. Cai, J. Zheng and Y. Dong, *Angew. Chem., Int. Ed.*, 2020, **59**, 16054–16060.
45 J. Wang, X. Gu, H. Ma, Q. Peng, X. Huang, X. Zheng, S. Sung, G. Shan, J. Lam, Z. Shuai and B. Tang, *Nat. Commun.*, 2018, **9**, 2963.
46 X. Dou, T. Zhu, Z. Wang, W. Sun, Y. Lai, K. Sui, Y. Tan, Y. Zhang and W. Yuan, *Adv. Mater.*, 2020, **32**, 2004768.
47 O. Bolton, K. Lee, H. Kim, K. Lin and J. Kim, *Nat. Chem.*, 2011, **3**, 205–210.
48 C. Sun, X. Ran, X. Wang, Z. Cheng, Q. Wu, S. Cai, L. Gu, N. Gan, H. Shi, Z. An, H. Shi and W. Huang, *J. Phys. Chem. Lett.*, 2018, **9**, 335–339.
49 X. Wang, H. Ma, M. Gu, C. Lin, N. Gan, Z. Xie, H. Wang, L. Bian, L. Fu, S. Cai, Z. Chi, W. Yao, Z. An, H. Shi and W. Huang, *Chem. Mater.*, 2019, **31**, 5584–5591.
50 L. Gu, H. Shi, L. Bian, M. Gu, K. Ling, X. Wang, H. Ma, S. Cai, W. Ning, L. Fu, H. Wang, S. Wang, Y. Gao, W. Yao, F. Huo, Y. Tao, Z. An, X. Liu and W. Huang, *Nat. Photonics*, 2019, **13**, 406–411.
51 S. Cai, H. Ma, H. Shi, H. Wang, X. Wang, L. Xiao, W. Ye, K. Huang, X. Cao, N. Gan, C. Ma, M. Gu, L. Song, H. Xu, Y. Tao, C. Zhang, W. Yao, Z. An and W. Huang, *Nat. Commun.*, 2019, **10**, 4247.
52 S. Kuila and S. George, *Angew. Chem., Int. Ed.*, 2020, **59**, 9393–9397.
53 D. Wang, J. Gong, Y. Xiong, H. Wu, Z. Zhao, D. Wang and B. Tang, *Adv. Funct. Mater.*, 2023, **33**, 2208895.
54 H. Peng, G. Xie, Y. Cao, L. Zhang, X. Yan, X. Zhang, S. Miao, Y. Tao, H. Li, C. Zheng, W. Huang and R. Chen, *Sci. Adv.*, 2022, **8**, eabk2925.
55 L. Gu, W. Ye, X. Liang, A. Lv, H. Ma, M. Singh, W. Jia, Z. Shen, Y. Guo, Y. Gao, H. Chen, D. Wang, Y. Wu, J. Liu, H. Wang, Y. Zheng, Z. An, W. Huang and Y. Zhao, *J. Am. Chem. Soc.*, 2021, **143**, 18527–18535.
56 Y. Zhang, Y. Su, H. Wu, Z. Wang, C. Wang, Y. Zheng, X. Zheng, L. Gao, Q. Zhou, Y. Yang, X. Chen, C. Yang and Y. Zhao, *J. Am. Chem. Soc.*, 2021, **143**, 13675–13685.
57 Y. Zhang, Q. Sun, L. Yue, Y. Wang, S. Cui, H. Zhang, S. Xue and W. Yang, *Adv. Sci.*, 2021, **9**, 2103402.
58 S. Sun, Y. Zhu, T. Li, G. Wang, F. Yin, F. Li, F. Tao, L. Wang and G. Li, *Chem. Eng. J.*, 2024, **485**, 149751.
59 H. Ju, H. Zhang, L. Hou, M. Zuo, M. Du, F. Huang, Q. Zheng and Z. L. Wu, *J. Am. Chem. Soc.*, 2023, **145**, 3763–3773.
60 J. Wei, M. Zhu, T. Du, J. Li, P. Dai, C. Liu, J. Duan, S. Liu, X. Zhou, S. Zhang, L. Guo, H. Wang, Y. Ma, W. Huang and Q. Zhao, *Nat. Commun.*, 2023, **14**, 4839.
61 G. Li, F. Du, H. Wang and R. Bai, *React. Funct. Polym.*, 2014, **75**, 75–80.
62 S. Yuan, Y. Zhang, J. Chen, Y. Yu, L. Yue, Q. Sun, H. Zhang, S. Xue and W. Yang, *Adv. Opt. Mater.*, 2022, **10**, 2200090.
63 T. Li, S. Sun, Y. Zhou, Z. Wang, X. Wang, S. Yang, F. Tao, L. Wang and G. Li, *Mater. Today Chem.*, 2025, **48**, 102915.
64 Z. Yang, C. Xu, W. Li, Z. Mao, X. Ge, Q. Huang, H. Deng, J. Zhao, F. Gu, Y. Zhang and Z. Chi, *Angew. Chem., Int. Ed.*, 2020, **59**, 17451–17455.
65 J. Yuan, R. Chen, X. Tang, Y. Tao, S. Xu, L. Jin, C. Chen, X. Zhou, C. Zheng and W. Huang, *Chem. Sci.*, 2019, **10**, 5031–5038.
66 W. Zhao, Z. He and B. Tang, *Nat. Rev. Mater.*, 2020, **5**, 869–885.
67 F. Peng, C. Qiu, P. Wu, S. Hu, P. Chen, X. Li, M. Li, Z. Chen, S. Su and H. Qi, *Adv. Opt. Mater.*, 2024, **12**, 2401419.
68 T. Ono, K. Kimura, M. Ihara, Y. Yamanaka, M. Sasaki, H. Mori and Y. Hisaeda, *Chem.–Eur. J.*, 2021, **27**, 9535–9541.
69 Y. Zhang, M. Gutiérrez, A. Chaudhari and J. Tan, *ACS Appl. Mater. Interfaces*, 2020, **12**, 37477–37488.